Technical Report
1063

Calculation of Resident Space Object Color Temperature and Emissivity-Area from MSX SPIRIT III Infrared Data: Emissive Reference Sphere Results

R.L. Lambour

13 September 2002

Lincoln Laboratory

MASSACHUSETTS INSTITUTE OF TECHNOLOGY

LEXINGTON, MASSACHUSETTS

A DA 406599
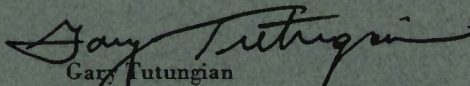
The ESC Public Affairs Office has reviewed this report, and it is releasable to the National Technical Information Service, where it will be available to the general public, including foreign nationals.

This technical report has been reviewed and is approved for publication.

FOR THE COMMANDER

Gary Tutungian
Administrative Contracting Officer
Plans and Programs Directorate
Contracted Support Management

Massachusetts Institute of Technology
Lincoln Laboratory

Calculation of Resident Space Object Color Temperature and Emissivity-Area from MSX SPIRIT III Infrared Data: Emissive Reference Sphere Results

R.L. Lambour
Group 91

Technical Report 1063

13 September 2002

Lexington   Massachusetts

ABSTRACT

This report discusses the calculation of color temperature and emissivity-area product from resident space object (RSO) observations that were obtained during a series of surveillance experiments carried out with the Midcourse Space Experiment (MSX) spacecraft. During these experiments, simultaneous infrared and visible-band data were collected with the SPIRIT III LWIR infrared radiometer and the Space-Based Visible (SBV) instruments, respectively. Algorithms were developed for the SPIRIT III Data Reduction pipeline that allow calculation of color temperature and emissivity-area product for RSOs given that the RSO was observed in at least two wavelength bands. This report discusses the algorithms and characterizes their accuracy using data taken on five emissive reference spheres that were deployed from the satellite over the lifetime of the SPIRIT III instrument.

TABLE OF CONTENTS

LIST OF ILLUSTRATIONS

LIST OF TABLES

1. INTRODUCTION

The Midcourse Space Experiment (MSX) spacecraft was launched in April 1996 into a circular, 898-km, sun-synchronous orbit with an inclination of 99 deg. The primary purpose of the satellite was to collect target and background phenomenology data in order to facilitate detection, acquisition, and tracking of ballistic missile targets in midcourse flight, as well as discrimination of lethal and non-lethal ballistic missile targets. The spacecraft is equipped with a suite of optical instruments that make measurements from the far ultraviolet (110 nm) to the long wave infrared (26 μm) region of the spectrum. The optical instruments are the SPatial InfraRed and Imaging Telescope (SPIRIT) III, a cryogenically-cooled radiometer and interferometer, the Space-Based Visible (SBV) camera, and the Ultraviolet/Visible Imaging and Spectrographic Imaging (UVISI) sensors.

During the 10-month period before the SPIRIT III cryogen was exhausted (April 1996 through February 1997), use of the spacecraft was shared between eight Principal Investigator (PI) groups. This time period is referred to as MSX Phase I data collection or simply as Phase I. The Surveillance PI group executed fifteen experiments (data collection events or DCEs) during Phase I. The experiments utilized SPIRIT III and SBV simultaneously and are summarized in Reference 1. Five different types of experiments were run, all of which collected data simultaneously in the infrared (IR) and visible bands.

The primary objective of the experiments was to examine the multi-band IR and visible data for its utility in supporting Space Object Identification (SOI) and space surveillance. The objective of SOI is draw conclusions about RSOs (what it is and what it is doing) using the observed and inferred characteristics. Those characteristics include the RSOs temperature, area, emissivity, absorptivity, reflectivity, and temporal trends. The Lincoln Laboratory SPIRIT III Data Reduction pipeline[1] calculates two-color target temperature and emissivity-area product (εA) routinely for all RSO observations that have been correlated to known objects. This report describes the algorithms utilized by the pipeline to calculate T and εA and discusses the accuracy to which they can be detrmined. Section 2 describes the SPIRIT III radiometer. Section 3 presents the physics behind the determination of an RSOs temperature and its IR signature. Section 4 presents the two-color temperature calculation algorithm and Section 5 discusses the accuracy to which it can be determined. Section 6 describes the calculation and accuracy of εA. Section 7 presents a discussion of the results and Section 8 presents the conclusions of this report.

2. THE SPIRIT III RADIOMETER

The SPIRIT III sensor is the primary sensor on MSX. It was designed and built at the Utah State University Space Dynamics Laboratory in Logan, Utah. The telescope covers the spectrum from the mid-wave IR (MWIR) to the long-wave infrared (LWIR). SPIRIT III consists of an off-axis, high stray-light rejection, reimaging telescope with a 37-cm diameter aperture, a 6-band scanning radiometer, and a 6-channel, high-resolution interferometer-spectrometer, all of which are cooled to cryogenic temperatures (~10-13 °K) by a dewar/heat exchanger which was filled with solid hydrogen. The cryogen lasted 10 months once the spacecraft was on orbit.

The interferometer was not used during the space surveillance experiments and will not be discussed. The SPIRIT III radiometer is a line-scanning radiometer that measures IR radiation in 6 spectral bands that range from 4.2 – 26 μm and have a spatial resolution of 90 μrad. The wavelength bands are listed in Table 1. The wavelength bands that were processed for the surveillance experiments are shown in bold type. A bi-directional scan mirror is used to build up an image over a variable field of regard that is centered on the telescope boresight. The radiometer scan mirror can remain fixed or can operate at a constant scan rate of 0.46 deg/sec with a selectable field of regard of 1 x 0.75°, 1 x 1.5°, or 1 x 3°. Therefore, the time required to build up a scan varies from 1.63 sec to 6.52 sec, depending on the scan mode selected. The scan mode used during the surveillance experiments generated 1 x 1.5° scans at a "frame rate" of 1 scan every 3.26 sec. These individual scans are referred to as scenes.

The integration time (the time required to read out all 192 rows of the array columns) was also selectable. The surveillance experiments used a mirror scan mode with an integration time of ~2.7 msec. Given the scan rate of the mirror, this produced an effective dwell time on a pixel of ~11 msec. Thus, this mode of operation over-sampled the field of regard by about a factor of 4 (~4 samples were collected for any point in the field of regard). This allowed the instrument to build up enough SNR to detect relatively faint objects. The sensitivity of each radiometer band is characterized in Table 1 by the noise equivalent irradiance (NEI). Additional details on the radiometer can be found in References 2 and 3.

The radiometer underwent extensive ground and on-orbit calibration in order to determine calibration quantities (e.g., NEI, responsivity, radiometer pixel linearity, etc.). It is beyond the scope of this report to describe the calibration procedures and activities. For additional information, the reader is referred to References 4 and 5 and the references therein.

TABLE 1
SPIRIT III Band Characteristics (FWTM[§])

Spectral Band	Wavelength (μm)	NEI (W/cm^2)*
A	**6.03-10.92**	**3.2×10^{-18}**
B1	4.21-4.37	4.5×10^{-17}
B2	4.23-4.47	3.7×10^{-17}
C	**11.05-13.27**	**1.4×10^{-17}**
D	**13.32-16.05**	**5.4×10^{-18}**
E	18.03-26.79	1.5×10^{-17}

*FP Temperature = 12 K
[§]Full-width tenth maximum

3. RSO TEMPERATURE AND IR SIGNATURE

The temperature of an RSO is influenced by a number of factors that are diagrammed in Figure 1. Consider the concept of instantaneous thermal equilibrium, in which the amount of energy emitted by the RSO is, at any instant, equal to the amount of energy absorbed. This situation represents the conservation of energy. The power (energy per unit time) incident on the surface of the RSO can be written as:

$$\text{Incident Power} = A_p\Phi_{\text{sun}} + aFA_p\Phi_{\text{sun}} + FA_p\Phi_{\text{Earth}} + Q_{int} \tag{1}$$

where F is the Earth view factor, A_p is the *projected* area of the RSO (e.g., πr^2 for a sphere), Φ_{sun} is the energy flux incident on the RSO from the Sun (~1360 W/m^2 at the Earth), Φ_{Earth} is the energy flux incident on the RSO due to the warm Earth, a is the albedo of the Earth scene that is visible to the RSO, and Q_{int} is a term describing the internal heat generation of the RSO. The Earth view factor is the fraction of 4π solid angle subtended by the Earth at the location of the RSO. The first term on the right of the equal sign represents the power incident from direct solar illumination. The second term represents the power incident on the RSO due to reflection of solar illumination by the Earth. The albedo, a, represents the reflectivity of the Earth averaged over the entire Earth-scene visible to the RSO. The albedo is highly variable, depending on the visible terrain type (e.g., snow, desert, forest, ocean, etc.) and the amount of cloud cover. The Earth's albedo can range from 0.08 to 0.8, although 0.3 is an accepted average value[6]. The third term represents the contribution of upwelling, terrestrial thermal (long-wave IR) radiation (Earthshine) incident on the RSO due to its proximity to the warm Earth. This upwelling power is principally dependent on the temperature of the Earth's surface and atmosphere and the amount of cloud cover[7]. The final term represents the contribution of internal heat sources. The power absorbed by the RSO surface is a fraction of the incident power:

$$\text{Absorbed Power} = \alpha_s(A_p\Phi_{\text{sun}} + aFA_p\Phi_{\text{sun}} + gFA_p\Phi_{\text{Earth}}) + \alpha_i Q_{int} \tag{2}$$

where α_s represents the solar absorptivity coefficient for the RSO surface material. In general, this coefficient varies with wavelength; the relation in Equation (2) assumes that the RSO is a graybody. A graybody is an imperfect Planckian radiator for which the absorptivity and emissivity are independent of wavelength. The graybody absorptivity and emissivity values are also less than 1. We have assumed in Equation (2) that the absorptivity of the interior surface, α_i, may be different from the solar absorptivity of the exterior surface. Equation two also includes a factor, g, where $g\alpha_s = \alpha_{ir}$, the absorptivity at infrared wavelengths (where Φ_{Earth} is largest). For a graybody, we assume $g = 1$.
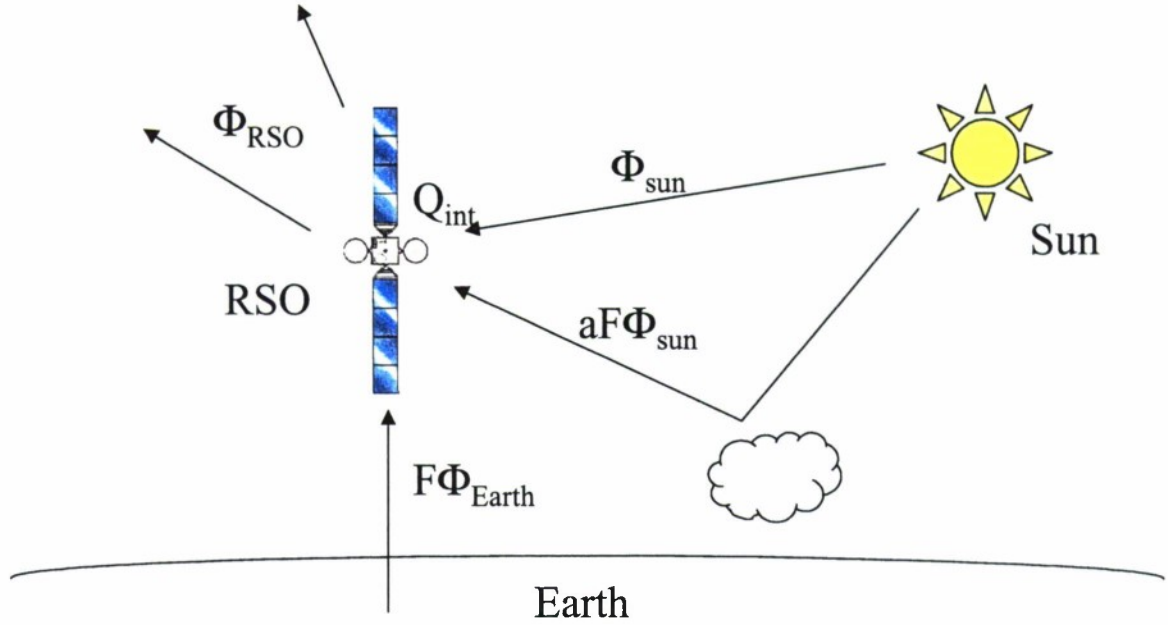
Figure 1. Diagram of RSO thermal environment. The energy flux from each source is shown, as well as the energy flux from the radiating RSO.

The power emitted from the RSO surface can be approximated as:

$$\text{Emitted Power} = A_s \Phi_{RSO} = \varepsilon_{ir} A_s \sigma T^4 \tag{3}$$

where A_s is the *total* surface area of the RSO (e.g., $4\pi r^2$ for a sphere), ε_{ir} is the infrared emissivity of the RSO surface material, σ is the Stefan-Boltzmann constant (5.67×10^{-8} J/m²-K⁴), and T is the temperature of the RSO. In general, the emissivity varies with wavelength, but Equation (3) assumes that the RSO is a graybody.

Assuming thermal equilibrium, Equations (2) and (3) can be equated. Solving for the temperature shows that the equilibrium temperature of an RSO depends upon its cross-sectional area, and the optical properties of its surface material.

The temperature of the RSO is estimated by examination of the RSO signature observed by the SPIRIT III radiometer. There are two components to the RSO IR signature: self-emitted radiation and reflected IR radiation. The sources contributing the self-emitted component of the signature were described in Equation (3). The reflected component of the signature is predominantly due to reflection of upwelling Earthshine from the surface of the RSO. This is demonstrated in Figure 2. The calculation in figure 2 assumes that the Earthshine is well represented by a 280 °K blackbody for bands A and C, and by a 240 °K blackbody for band D[8]. The reflected Earthshine component also depends upon the reflectivity of the RSO surface ($\rho = 1-\alpha$) and all of the factors affecting the amplitude of the upwelling Earthshine.

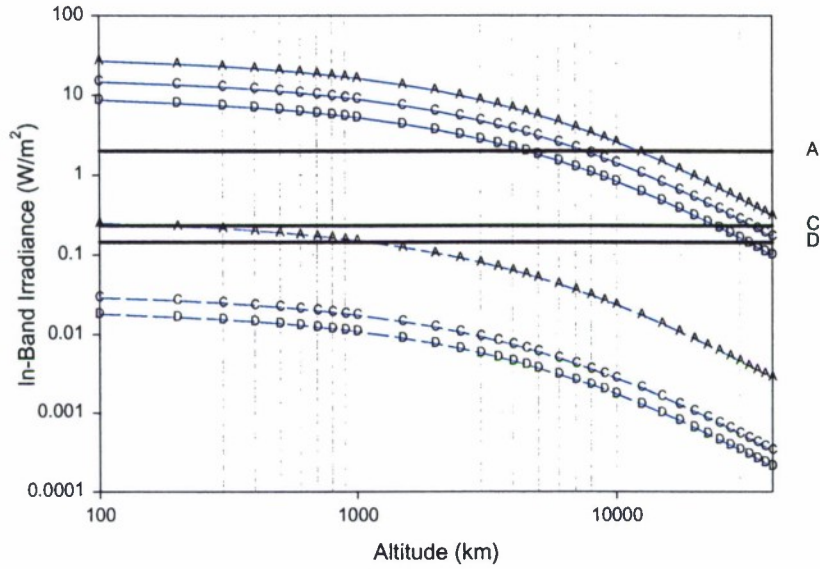*Figure 2. Comparison of energy flux reflected from a spherical graybody RSO as a function of altitude for three sources: Earthshine (thin solid lines) and solar radiation reflected off the Earth (dashed lines), and direct solar illumination (thick solid lines). Each band is identified by a letter and corresponds to the wavebands listed in Table 1. Each waveband is assumed to be square. RSO properties are listed in Table 2. The reflectivity is 1-α_s = 0.5.*

The relative importance of self-emitted radiation and reflected Earthshine can be estimated by constructing a simple signature model. Under the previous graybody assumption, Equations (2) and (3) are solved for an equilibrium temperature:

$$T_{eq} = \left[\frac{\alpha_s A_p \left(\Phi_{sun} + aF\Phi_{sun} + F\Phi_{Earth} \right) + \alpha_i Q_{int}}{\varepsilon_{ir} A_s \sigma} \right]^{1/4} \tag{4}$$

which is then used to calculate a self-emitted energy flux $= \sigma T_{eq}^4$. The upwelling Earthshine energy flux at the RSO is calculated from $F\Phi_{Earth}$, where the same assumption about the temperature of the Earth used to produce Figure 2 was used to calculate Φ_{Earth} in the three wavelength bands. The view factor can be approximated as:

$$F = \frac{\Omega}{4\pi} = \frac{1}{2} \left(1 - \cos\Theta \right); \Theta = \arcsin\left(\frac{r}{r+h} \right) \tag{5}$$

where r is the radius of the Earth (6378 km) and h is the RSO altitude[9]. Figure 3 shows the result of a calculation assuming a graybody spherical target and the parameters shown in Table 2. The plot shows the ratio of self-emitted radiation (W/m^2) to incident upwelling Earthshine (W/m^2), as a function of altitude for the SPIRIT III A, C, and D wavebands (cf. Table 1). The Earthshine reflected from the RSO will be a fraction, ρ, of the Earthshine incident on the RSO; therefore Figure 3 represents an upper limit on the reflected Earthshine portion of the RSO signature. The reflected component of the signature is

7

inversely proportional to the distance between the Earth and the RSO. Therefore, the contribution of the reflected Earthshine is largest for RSO that are near the Earth.

The internal source term, Q_{int}, was neglected in the previous calculation. This assumption is good for the reference spheres, as they have no internal heat source. This assumption is probably adequate for RSOs in general. Debris and rocket bodies have no internal heat sources. Payloads are usually covered with thermal insulation blankets that facilitate internal temperature control to within ±5 °K, with a common internal temperature in the range of 288-293 °K[10]. The thermal insulation provides excellent thermal isolation of the interior of the spacecraft from the exterior environment. The amount of heat that passes through an insulation layer can be estimated by:

$$q = \varepsilon_{eff}\sigma(T^4_{hot} - T^4_{cold})$$ (6)

where ε_{eff} is the effective emissivity of modern multi-layer insulation (about 0.05[10]), T_{hot} is the temperature of the hot boundary of the insulation blanket, and T_{cold} is the temperature of the cold boundary of the blanket[11]. If we consider an aluminized Kapton insulation blanket with a flat plate shape ($\alpha_s/\varepsilon_{ir} = 0.67$; $T_{eq} = 302$ °K)[12] and assume that the cold layer of the blanket is at the same temperature as the interior of the RSO (~288 °K), then the insulation actually lets external heat in. The internal source term does not contribute significantly to the signature of the object. This result is dependent upon the exact optical properties of the insulation blankets, but provides a reasonable estimate of the transfer of energy between the RSO interior and the exterior environment.

TABLE 2
Signature Model Parameters
For a Spherical Graybody

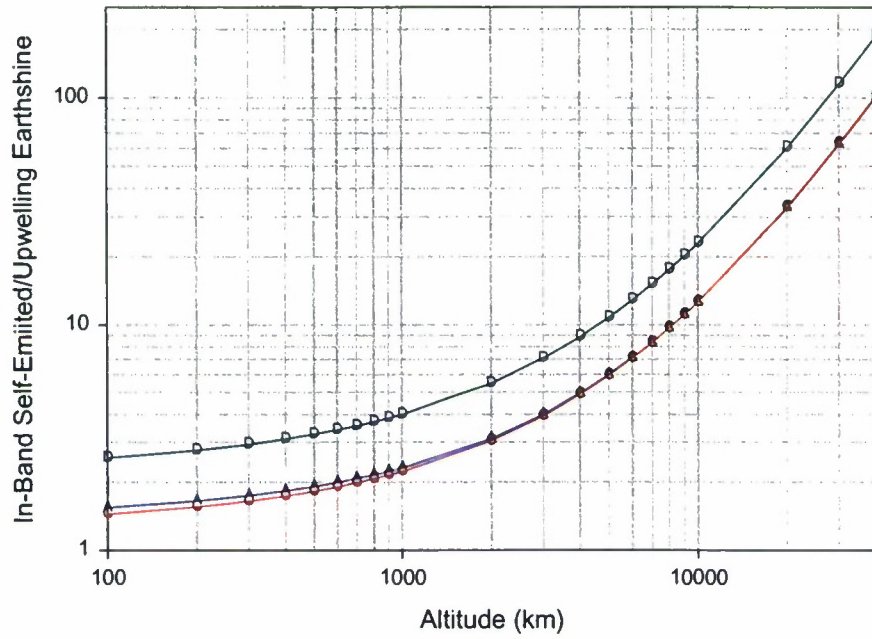|	
α_s	0.5
ε_{ir}	0.5
Φ_{sun}	1360 W/m^2
A_p/A_s	¼ (sphere)

Figure 3. Ratio of self-emitted flux to incident upwelling Earthshine, as a function of altitude and wavelength band (A, C, and D). Each spectral band is marked by its letter designation; A and C overlap. The RSO is assumed to be a spherical graybody.

4. CALCULATION OF COLOR TEMPERATURE FROM SPIRIT III IR DATA

A common method for calculating the temperature of a remote object is to construct a ratio of the flux output from two bands of a multi-color sensor, and this approach is taken with the SPIRIT III data. Given a few assumptions about the nature of the observed RSO, this ratio can be uniquely related to the temperature of the target. The temperature so calculated is referred to as the color temperature. The procedure used is shown in Figure 4. The SPIRIT III IR data arrived at the Surveillance Data Analysis Center in raw form (uncorrected counts). The data were processed with the SPIRIT III CONVERT software in order to transform the raw telemetry to calibrated engineering units and to identify and extract the irradiances (W/cm^2) and positions of the observed point sources. A set of post-CONVERT processing filters identified which of the point sources were RSOs and correlated them with the known RSO catalog. This data processing chain is known as the Lincoln Laboratory SPIRIT III Data Reduction Pipeline. The pipeline is discussed in Reference 1. The observations returned from the pipeline contain the RSO object number, its position in inertial space (right ascension and declination), and the observed in-band irradiance (W/cm^2 at the instrument) for bands A, C, and D for those point sources that were correlated with the RSO catalog[1]. Three in-band irradiances allows two band ratios to be constructed (A/C and A/D), in principle (cf., Fig 4). However, the RSO signal in band C was sometimes very weak, in which case only the A/D-band ratio could be calculated. Note that we have no *a priori* information regarding the target's temperature; the two-dimensional nature of Fig. 4 requires that the points be placed somewhere. Second, the observed band ratio(s) is compared to a theoretical estimate of the band ratio(s) as a function of the target's temperature. This comparison allows the estimated temperature of the target RSO to be quickly determined by interpolation (cf. Fig. 4). We did not design this algorithm to make use of the band E data because this waveband had a relatively poor calibration[13] and we believe the resulting color temperatures would be of poor quality. A future report will address the utility of calculating color temperatures using the band E data.
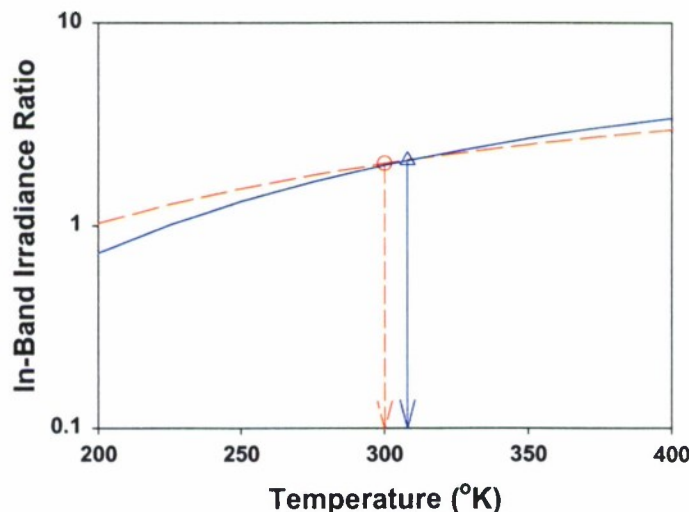

Figure 4. Observed band ratios A/C (circle) and A/D (triangle) compared with theoretical band ratios (solid lines; see text). Interpolation of RSO temperature from the theoretical curves is represented by the two arrows. In this example, the A/C temperature is 300 °K and the A/D temperature is 308 °K.

The assumptions involved in estimating the band ratio(s) for the RSO target warrant discussion. The observed in-band irradiance is the spectral irradiance of the object integrated over the waveband of interest:

$$I_i = \frac{A_p}{R^2} \int_0^\infty \varepsilon_{ir}(\lambda) RSR_i(\lambda) B(\lambda, T) d\lambda \tag{7}$$

where I_i is the irradiance in band i, R is the range to the RSO, $RSR_i(\lambda)$ is the relative spectral responsivity of band i (zero for wavelengths outside the band of interest), and $B(\lambda,T)$ is the spectral irradiance of the RSO. The relative spectral responsivity incorporates all of the effects on the RSO signature due to the optics of the observing instrument (e.g., spectral responsivity, transmission coefficient of the optics, etc.). The RSR is known for each band due to ground and on-orbit calibration[14], but the other quantities are generally unknown (R is known only for correlated objects). Therefore, it is usually quite difficult to invert Equation (7) and obtain information about the RSO.

Constructing a band ratio eliminates the dependence on A_p and R, since those are the same for each band, but leaves the dependences on the unknown emissivity and spectral irradiance of the target. Since the target is assumed to be a graybody, its spectral irradiance is Planckian:

$$B(\lambda, T) = \frac{2\pi h c^2}{\lambda^5 \left(e^{\frac{hc}{\lambda k T}} - 1 \right)} \tag{8}$$

where h is Planck's constant (6.63×10^{-34} J-s), c is the speed of light (2.998×10^8 m/s), and k is Boltzmann's constant (1.38×10^{-23} J/K). The graybody assumption also means that the emissivity is a constant across wavebands; therefore, when the band ratio is formed, the emissivity cancels out. The remaining function implicity depends only on temperature and is easily tabulated:

$$R_{ij} = \frac{\int_0^\infty RSR_i(\lambda) B(\lambda, T) d\lambda}{\int_0^\infty RSR_j(\lambda) B(\lambda, T) d\lambda} \tag{9}$$

The ratios R_{AC} and R_{AD} were calculated using these assumptions, in 5-degree increments, for the range of 100-3000 °K. These ratios are compared to the observed band ratios to derive the RSO color temperature (cf., Fig. 4). Therefore, the color temperatures are those that the target would have assuming that it is a graybody, and that all of the observed signature is due to the thermal self-emission of the target. The consequences of these assumptions will be discussed later.

Another method of estimating the RSO temperature is to calculate the temperature of an ideal blackbody whose radiant energy is equivalent to the observed radiant energy. This is called the brightness temperature. The brightness temperature is typically calculated at a specific wavelength; however, for our purposes, we define an in-band brightness temperature as the temperature of an ideal blackbody whose in-band radiant energy is equivalent to the observed in-band radiant energy. If an ideal blackbody is observed by a perfect sensor with square wavebands, the brightness and color temperatures will be equivalent and will be equal to the true temperature of the object. If the sensor has non-square

wavebands, then given that we know the spectral response of the sensor wavelength bands and that we have measurements of the radiant energy of a target in those bands, the accuracy to which the brightness temperature can be determined depends upon the overall accuracy of the measured radiant energy. The accuracy of this measurement depends in turn upon the calibration of the instrument and the noise properties of the instrument and the background scene against which the target is observed. For a sensor with small measurement errors, the deviation of the brightness temperature from the true temperature should be correspondingly small. If the target is not a blackbody ($\varepsilon_{ir} < 1$), the estimated brightness temperature will underestimate the true temperature of the object. For a non-black target the color temperature will be altered by the ratio of $\varepsilon_1/\varepsilon_2$ (if $\varepsilon_1 \neq \varepsilon_2$) where ε_i is the graybody emissivity in band i. This could result in an under/overestimation of the target temperature.

5. ACCURACY OF THE COLOR TEMPERATURE DETERMINATION

The best possible test for the temperature determination algorithm is to calculate the temperature of a target for which truth values are available. The MSX emissive reference sphere experiments provide such a truth reference. Five experiments were carried out over the 10-month lifetime of the SPIRIT-III instrument; each involved the deployment of a 2-cm diameter solid aluminum sphere with an emissive, Martin Black coating. The spheres were used to calibrate the SPIRIT radiometer. The spheres and their deployment scenarios were designed so that their IR signatures would be well characterized, essentially behaving as near-ideal blackbodies ($\alpha_s = \varepsilon_{ir} = 0.95$). The experiments probed the entire dynamic range of the SPIRIT III radiometer, as the spheres moved away from the MSX spacecraft. The details on the reference sphere experiments are summarized in Table 3.

TABLE 3
MSX Emissive Reference Sphere Experiment Parameters

Sphere	Deploy Date	Initial Temp (K)	Deploy Velocity (m/s)
1	1996:238:13:34	259.5	14.03
2	1996:258:11:13	259.2	14.40
3	1996:327:09:49	258.9	13.66
4	1996:354:13:05	258.9	14.60
5	1997:051:13:18	258.3	14.20

The Data Certification and Technology Transfer (DCATT) PI group carried out the reference sphere experiments. We obtained the observed in-band irradiances from bands A, C, D, and E and the estimated MSX-to-sphere ranges for all 5 experiments from the DCATT PI group. The irradiances were output of the SPIRIT III CONVERT data reduction software package (Version 6.2.1); see Reference 1 and the references therein for more details on the CONVERT software and processing. In addition, we obtained truth values for the sphere temperatures and their in-band irradiances from the DCATT group. An example of the reference sphere observations is shown in Figure 5.

The truth values for the spheres' temperatures and irradiances were the result of a significant modeling effort carried out by MIT Lincoln Laboratory[15-16] and the DCATT group[13, 17-18]. The models characterized the spheres' thermal environments, and consisted of three components: incident solar flux, incident solar flux reflected from the Earth, and incident upwelling Earthshine (cf., Equation 1). The details of the model are covered in the aforementioned references. We note that the DCATT model took the variation of emissivity with wavelength into account. The 1-sigma error in the reference temperature model is estimated to be < 1.5 K[17].
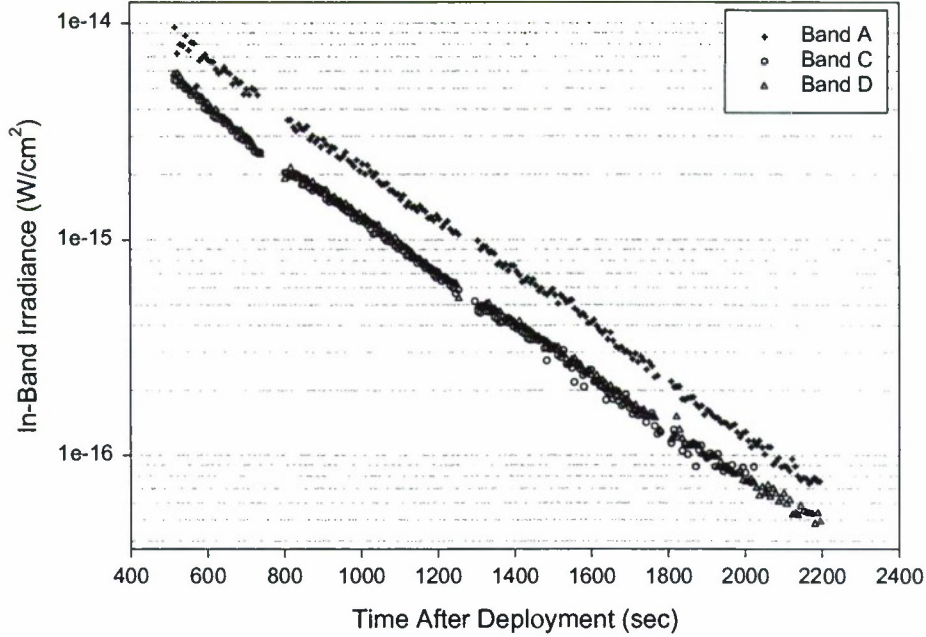
Figure 5. In-band irradiance values observed by SPIRIT III during the first emissive reference sphere calibration experiment.

We used the DCATT-supplied irradiance observations and our temperature determination algorithm to derive color temperature histories, using the A/C and A/D band ratios, for each of the reference spheres. In each scene the A, C, and D irradiances generally had slightly different time tags, so the observed irradiances were interpolated to facilitate formation of the band ratios with a common time tag. The difference between the color temperature and the truth model was then calculated for each of the spheres. The data were screened for three-sigma outliers. The mean difference and the standard deviation of the differences were calculated; these represent a bias and precision of the temperature determination, respectively.

Figure 6 shows the color temperature that we calculated for the first emissive reference sphere (ERS). The triangles represent the A/C temperature, and circles represent the A/D temperature. The temperature of the sphere 400 seconds after deployment is about 270 °K, which is near the deploy temperature of 259.5 °K. There are no data plotted prior to 400 seconds, because the pixels of the radiometer were saturated, rendering the irradiance values useless. There are three gaps in the data due to the execution of routines designed to measure the dark current of the radiometer focal planes (see also Fig. 5). The sphere was sunlit when deployed but crossed the terminator at ~1600 seconds after deployment; the temperature of the sphere rose while sunlit and fell after the terminator crossing, as expected. The computed color temperatures are reasonable; a sunlit sphere in thermal equilibrium, with $\alpha = \varepsilon$, will have an equilibrium temperature of 278.5 °K[19]. It is easy to show, using the model described in Section 3, that due to the proximity of the sphere to the Earth, the sphere will warm to an equilibrium

16

temperature of ~287.5 °K; this is similar to the temperature attained by the sphere before it entered eclipse. The A/C and A/D color temperatures agree well with each other during the event.
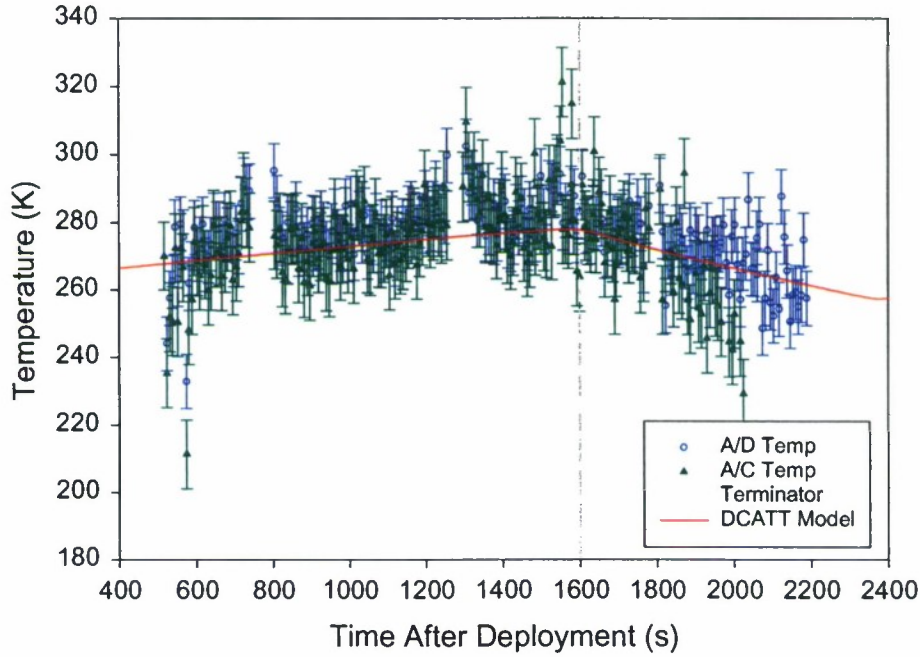

Figure 6. "Observed" temperatures for ERS-1 as calculated by our algorithm. The two temperature estimates agree nicely and behave as expected. The error bars represent the 1-sigma temperature error as described in the text and in Table 4. The sphere heats up while illuminated and cools off after it crosses the terminator (~1600 sec after deployment).

Figure 7 shows the three-sigma-screened temperature residuals ($T_{color} - T_{truth}$) for ERS-1. The mean residuals for the A/C and A/D temperatures are 0.55 and 4.21 °K, respectively. There is a small positive bias in the temperature. The standard deviations, or precisions, for the A/C and A/D residuals are 10.16 and 6.77 °K, respectively. The bias and precision are added, in quadrature, to provide an estimate of the total error in the calculated temperature over the entire track:

$$Error = \sqrt{Bias^2 + Precision^2} \qquad (10)$$

For ERS-1, the A/C and A/D temperature errors are 10.18 and 7.97 °K, respectively. The biases, precisions, and errors for ERS-1 and the other 4 reference spheres are presented in Table 4. A mean accuracy was calculated by weighting the accuracy for each sphere by the number of data points in the sphere track. Averaged over all 5 reference spheres, the mean A/C (A/D) temperature accuracy is 11.02 (9.32) °K. We believe that this accuracy conservatively represents the capability of the sensor, the CONVERT software, and the post-processing algorithms, combined. The number of data points used in the calculation of Table 4 and the remaining plots for spheres 2-5 appear in Appendix A.
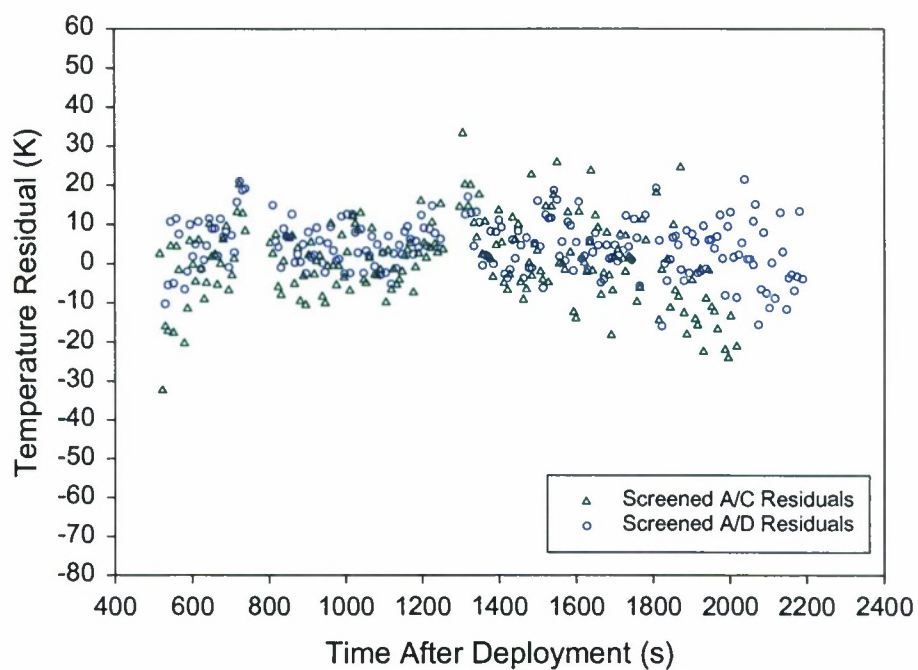
17

Figure 7. Temperature residuals for ERS-1. Three-sigma outliers have been screened from the data.

TABLE 4
Emissive Reference Sphere Temperature Accuracy

Sphere	A/C Bias (°K)	A/C Precision	A/C Error (°K)	A/D Bias (°K)	A/D Precision	A/D Error (°K)
ERS-1	0.55	10.16	10.18	4.21	6.77	7.97
ERS-2	3.24	10.95	11.42	7.67	6.34	9.95
ERS-3	4.17	10.90	11.67	5.07	10.87	11.99
ERS-4	1.06	10.23	10.28	4.31	10.09	10.97
ERS-5	-3.77	11.63	12.23	1.50	8.72	8.85

18

6. CALCULATION AND ACCURACY OF EMISSIVITY-AREA PRODUCT

In addition to estimating the color temperature of an RSO, we can use the SPIRIT III IR data to estimate the emissivity-projected-area product, εA_p, for an RSO. An interesting technique for extracting emissivity, area, and temperature of a target, using the IR signature observed by a 3-band LWIR sensor, has been developed[20]. However, it is not usually applicable in this work because we do not often have observations in three bands. This deficiency is due to the poor sensitivity of the SPIRIT III C band in mirror scan mode. Therfore, we adopted a simple algorithm, which was employed to calculate εA_p for RSOs detected by the IRAS satellite[12]. The emissivity-area may be estimated by setting the in-band brightness temperature equal to the color temperature and solving for εA_p[21]:

$$\varepsilon A_i = \frac{\pi R^2 I_i}{\int_0^\infty RSR_i(\lambda)B(\lambda, T_{obs})d\lambda} \tag{11}$$

In Equation (11) I_i is the observed irradiance in band i, R is the range to the target, T_{obs} is the color temperature calculated from the SPIRIT observations, and B is the Planck spectral irradiance defined in Equation (8). We estimated εA_p using the band A data. This algorithm required that a particular RSO observation be correlated to the RSO catalog (so that R was known) and that the RSO had been detected in at least two bands (so that color temperature could be estimated). The ratio in Equation (11) represents the emissivity-area product that the target would have assuming that it is a graybody emitter and that all of the observed radiation is due to the self-emission of the target.

The algorithm for determining εA_p was tested using the ERS data. We assume the emissivity-area product of the reference spheres is approximately equal to 0.000298 m². We have assumed that the area of the 2-cm spheres is well known and that the emissivity of the spheres was 0.95[17]. Figure 8 compares the εA_p estimates with the truth value for the first sphere. The estimates agree fairly well with the truth value. We calculated bias and precision values for each of the spheres in a manner similar to the way we calculated the bias and precision for the temperature. The biases and precisions were added in quadrature to obtain an estimate of the error in our calculation (cf., Equation 9). The error in the truth model, mentioned above, is very small and was neglected. The accuracy estimates appear in Table 5. For clarity, the residuals have been normalized to the true εA_p value for the spheres, and have been multiplied by 100 so that the numbers in Table 5 are percentages. For example, ERS-1 shows a bias of −9.7, showing that on average our εA_p estimates were ~10% low for this sphere. Table 5 shows that the emissivity-area estimates for the spheres are good to only 14-20%. The mean error, weighted by the number of measurements per track, is 16.8%. The εA_p residuals (calculated − truth values) for the five spheres are presented in Appendix B.
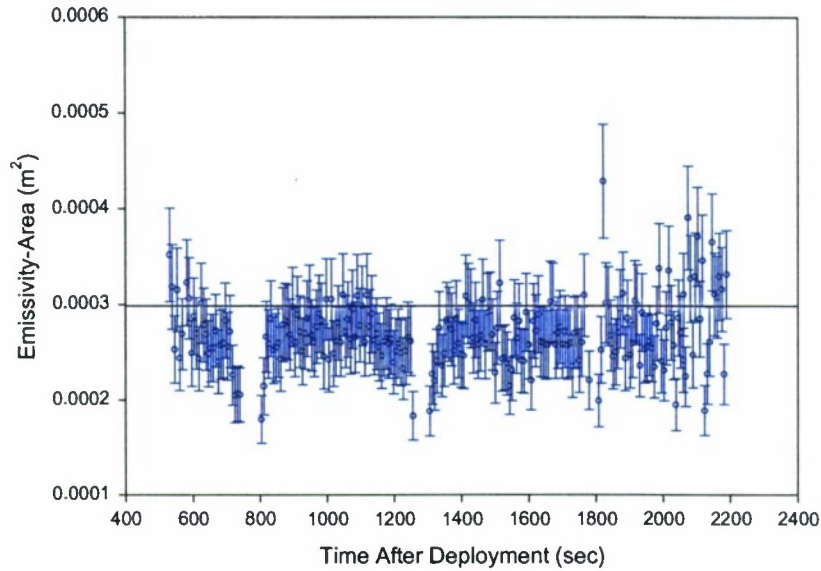
Figure 8. Estimated emissivity-area product for ERS-1. The solid black line is the truth value of 0.000298 m². The error bars represent the 1-sigma error in the estimates as described in the text and Table 5. These estimated were made using the SPIRIT III A-band irradiance data.

TABLE 5
Emissive Reference Sphere εA_p Error Estimates

Sphere	εA Bias (%)	εA Precision (%)	εA Error (%)
ERS-1	-9.7	11.6	15.1
ERS-2	-11.2	9.3	14.5
ERS-3	-6.2	19.1	20.1
ERS-4	-6.6	19.2	20.4
ERS-5	+4.5	16.4	17.0

The precision of the εA_p estimate and the total error in the estimate decrease with subsequent sphere deployments (exception: ERS-5). Therefore the band ratios exhibit increasing variation over the lifetime of the radiometer (this increased variation is also seen by looking at the color temperature errors as a function of time). This is presumably a result of the increase in the temperature of the radiometer focal plane (and thus focal plane noise) over the lifetime of the instrument. This increase in focal plane temperature, and the corresponding increase in focal plane noise, was apparently accounted for by the CONVERT software (cf., Ref. 1 and references therein) during data reduction. However, we know of no reasonable explanation for the increased variation in the band ratios with time other than an increase in focal plane noise. It is possible that the CONVERT process did not account for all of the variation in observed irradiance due to focal plane temperature changes.

We also note that the εA_p estimates tend to be biased low (exception: ERS-5); this is evident in Figure 8. If we assume the reflected Earthshine component of the sphere's signatures is negligible, which is a good assumption given the non-reflective nature of the spheres, this bias suggests that the estimated color temperatures were systematically high, or that the MSX-to-sphere ranges were systematically low (or both). The reference spheres were not tracked by the radars in the Space Surveillance Network, so we have no information regarding the actual time histories of MSX-to-sphere range to compare with our range estimates. Table 4 shows that a positive bias in the estimated color temperatures does exist. Assuming that there is no bias in the temperature determination algorithm, this temperature bias suggests that there is a positive bias in the band ratios or perhaps a uniform bias in the irradiance values that form the band ratios. We did not look into the issue of irradiance errors, but the DCATT PI group has and did not observe a systematic bias in either the band ratios or the irradiances for the reference spheres[13]. The temperature bias may also be a result of non-gray target behavior. A positive bias in the temperature can indicate that $\varepsilon_1 > \varepsilon_2$ rather than $\varepsilon_1 = \varepsilon_2$, where ε_1 is the spectral emissivity in the shorter wavelength band (band A in this case). In the case of the reference spheres, the graybody assumption is a good one in the 6-16 μm region of the spectrum, and the truth model accounted for the non-gray nature of the Martin Black coating in the other regions of the spectrum[17,18]. Therefore it seems most likely that the bias in temperature, which contributes to the bias in εA, is due to an unresolved bias in the color temperature calculation proceedure. We note that the weighted mean bias in the εA estimates is -5.45%. This may be explained by an MSX-to-sphere range which is systematically low by ~3%, or may be explained by a temperature which is systematically high by ~1%. For the ~280 °K spheres this is about 3 °K and is in fair agreement with the weighted mean A/D color temperature bias of 4.05 °K. Appendix C describes the derivation of these estimates.

7. DISCUSSION

Two significant assumptions were made in order to simplify the calculation of temperature and εA_p from the SPIRIT III irradiance data. First was the assumption that the target is a graybody. That assumption is an excellent one for the MSX Emissive Reference Spheres. In general, however, most space objects are probably not graybodies. The non-gray characteristics of a target at a specific temperature will cause the irradiances, and hence the irradiance ratios, to deviate from those of a gray target with the same temperature. The characterization of this behavior was examined briefly and will be expanded upon in the analysis of the remaining IR RSO data. These data will be discussed in a future report.

The second assumption is that all of the energy flux observed by the SPIRIT III radiometer was due to the thermal self-emission of the target. This assumption simplified the calculation of theoretical band ratios (cf. Section 4) by allowing us to neglect the contribution of reflected IR radiation to the targets' signature. The simple models presented in Section 3 demonstrate that this assumption is a good one for targets with altitudes greater than ~8000 km (cf., Figure 3), because at these altitudes, the ratio of self-emitted flux to upwelling Earthshine is greater than 10. At lower altitudes, the background source may contribute to the target signature given that the target is sufficiently reflective in the wavelength bands of interest. The reflected component will alter the observed irradiance ratio in such a way that the apparent temperature of the target falls between the true temperature of the target and the temperature characteristic of the background source[22]. Techniques have been developed to estimate and isolate the background contribution to the signature and thus produce more accurate target temperature estimates[20]. Those techniques were not applied to the ERS analysis for two reasons: 1.) The spheres are not reflective and the reflected component of their signature should be very small, and 2.) The technique mentioned requires good quality observations in at least 3 different wavelength bands. While we have good observations of the spheres in bands A, C, D, and E, this is not true in general for the other RSO targets observed during the Surveillance PI experiments which usually have observations only in bands A and D. Therefore, effort was not expended on the implementation of these three-band algorithms. Recall that we did not process band E due to poor radiometric calibration. We are investigating the utility of determining temperatures using band E data; should this band prove useful, we will readdress the utility of the three-band algorithms.

8. CONCLUSIONS

This report has described the process used by the SPIRIT III data reduction pipeline to calculate color temperature and emissivity-area product for correlated RSO observations obtained by the SPIRIT III radiometer during the surveillance PI DCEs. These algorithms were tested using the best truth reference available: the 5 emissive reference spheres deployed from the MSX over the lifetime of the SPIRIT instrument. The ERS data were fed into the temperature and εA algorithms to generate estimates of those quantities. The estimates were compared to truth models supplied by the DCATT PI team. We have determined empirically that the 1-sigma temperature error for the reference spheres is ~11°K for the A/C band ratio and ~9.3°K for the A/D band ratio. In addition, we have determined empirically that the pipeline fractional εA error for the reference spheres is ~17%. We believe that these errors conservatively represent the capability of the sensor, CONVERT software, and post-CONVERT processing algorithms. In addition, the utility of using band E data is being investigated and will be addressed in a future report.

REFERENCES

1.) Lambour, R. L., personal communication, 2000.

2.) *SPIRIT III Sensor User's Guide Revision 5*, SDL/92-041, Space Dynamics Laboratory, Utah State University, SDL/92-041, Logan, UT, May 1995.

3.) Bartschi, B. Y., D. E. Morse, and T. L. Woolston, The Spatial Infrared Imaging Telescope III, *John Hopkins APL Technical Digest*, vol. 17, No. 2, April-June 1996.

4.) *SPIRIT III Integrated Ground and On-Orbit Calibration Report in Support of Convert 5.0, Vols. 1 and 2*, SDL/97-056, Space Dynamics Laboratory, Utah State University, Logan, UT, March 1998.

5.) *Midcourse Space Experiment DCATT Experiment Plans, Vols. 1 and 2*, Ballistic Missile Defense Organization internal document, 16 August 1993.

6.) Peixoto, J. P., and A. H. Oort, *Physics of Climate*, American Institute of Physics, New York, NY, 1992.

7.) *Earth Albedo and Emitted Radiation*, NASA SP-8067, July 1971.

8.) Spitzberg, R. M., private communication, 2000.

9.) Sridharan, R., W. I. Beavers, E. M. Gaposchkin, R. L. Lambour, and J. E. Kansky, *A Case Study of Debris Characterization by Remote Sensing*, TR-1045A, MIT Lincoln Laboratory, Lexington, MA, 18 December 1998.

10.) Williamson, M., *The Communications Satellite*, Adam Hilger, New York, NY, 1990.

11.) Wertz, J. R., and W. J. Larson, *Space Mission Analysis and Design: Third Edition*, Microcosm, Torrance, CA, 1999.

12.) Gaposchkin, E. M., and R. J. Bergemann, Infrared Detections of Satellites with IRAS, Technical Report 1018, MIT Lincoln Laboratory, Lexington, MA, 26 September 1995.

13.) Taylor, S. –A., D. Morris, and C. Hamilton, *SPIRIT III CONVERT 5.0 Certification Report*, Report 6140-98-02-TR, Frontier Technology, Inc., Danvers, MA, April 1998.

14.) MSX SPIRIT III Web/FTP Site, http://www.spirit3.sdl.usu.edu.

15.) Kintner, E. C., and R. B. Sohn, personal communications, 1993.

16.) Kintner, E. C., P. D. Dolan II, and W. J. Jacobson, personal communication, 1995.

17.) Chalupa, J., W. K. Cobb, and T. L. Murdock, *Thermal History and Error Budget of an Emissive Calibration Sphere for a Space-Based IR Sensor, Part I: Gray-Body Analysis*, Report 1597-08-91-TR, General Research Corporation, Danvers, MA, December 1991.

18.) Chalupa, J., and C. L. Hamilton, *Thermal History and Error Budget of an Emissive Calibration Sphere for a Space-Based IR Sensor, Part II: Spectral Error Analysis*, Report 1945-03-93-TR, General Research Corporation, Danvers, MA, September 1993.

19.) Gaposchkin, E. M., and R. Sridharan, personal communication, 1991.

20.) Spitzberg, R. M., Parameter Estimation for Gray and Nongray Targets: Theory and Data Analysis, *Optical Engineering*, Vol. 33, No. 7, pp. 2418-29, 1994.

21.) Nicodemus, F. E., Radiometry, in *Applied Optics and Optical Engineering Volume IV*, R. Kingslake (ed.). Academic Press, New York, NY, 1967, pp. 293.

22.) Horman, M. H., Temperature analysis from multispectral infrared data, *Applied Optics*, Vol. 15, No. 9, pp. 2099-2104, 1976.

23.) Bevington, P. R., *Data Reduction and Error Analysis for the Physical Sciences*, McGraw-Hill Book Company, New York, NY, 1969.

APPENDIX A
EMISSIVE REFERENCE SPHERE TEMPERATURE PLOTS

The color temperature calculated by the SPIRIT III Data Reduction pipeline for reference sphere 1 (ERS-1) was presented in Section 5 of this report. This appendix presents the remaining reference sphere temperature data in the same format as Figures 7 and 8. First of all, Table A1 presents the number of data points available for the calculation of temperatures and emissivity-area product (εA).

TABLE A1
Number of Data Points Used to Derive
Temperature and εA for the Reference Spheres

Sphere	Band Ratio A/C	Band Ratio A/D
ERS-1	201	220
ERS-2	67	67
ERS-3	44	75
ERS-4	40	73
ERS-5	120	147

The top graph on each of the following pages is a plot of the observed temperature as a function of time with the A/C temperatures represented by triangles and the A/D temperatures represented by circles. The bottom plot shows the temperature residuals: the observed temperature minus the DCATT truth temperature. Three-sigma outliers have been removed from each data set. For convenient reference, Table 3 is reproduced in Table A2.

TABLE A2
MSX Emissive Reference Sphere Experiment Parameters

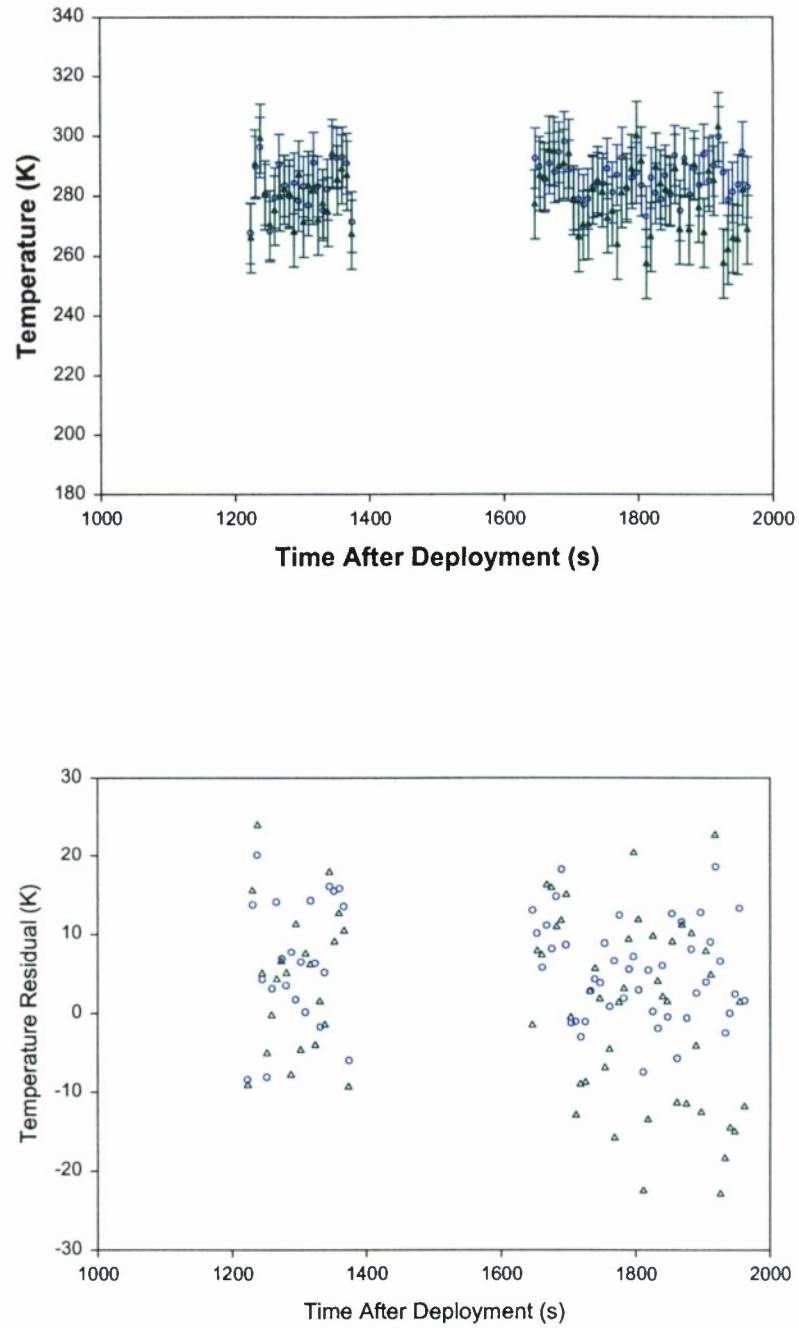| Sphere	Deploy Date	Initial Temp (K)	Deploy Velocity (m/s)
1	1996:238:13:34	259.5	14.03
2	1996:258:11:13	259.2	14.40
3	1996:327:09:49	258.9	13.66
4	1996:354:13:05	258.9	14.60
5	1997:051:13:18	258.3	14.20

29

Figure A1. Temperature history (top) and temperature residuals (bottom) for Emissive Reference Sphere #2. Bands A/C are represented by triangles and circles represent bands A/D.
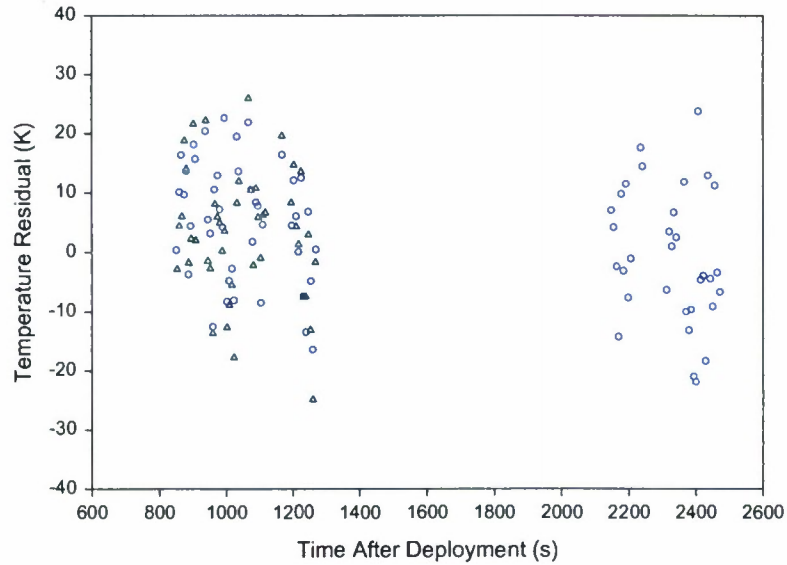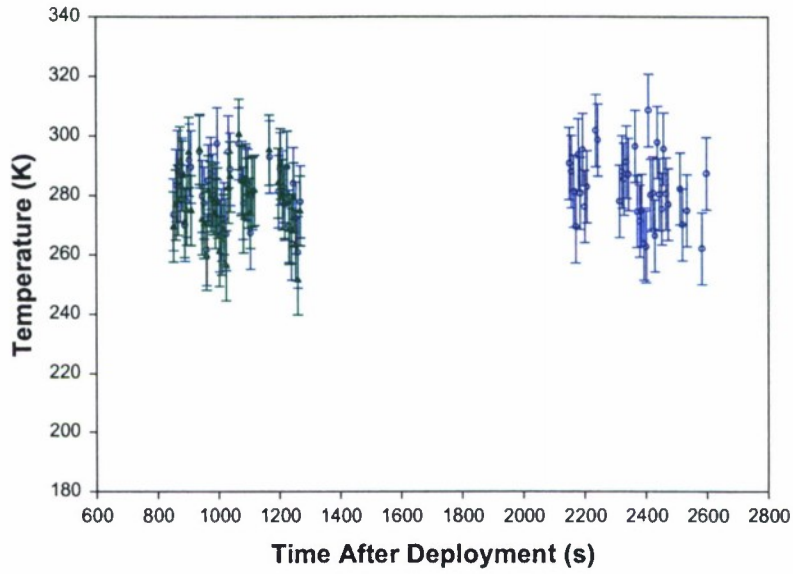
Figure A2. Temperature history (top) and temperature residuals (bottom) for Emissive Reference Sphere #3. Bands A/C are represented by triangles and circles represent bands A/D.
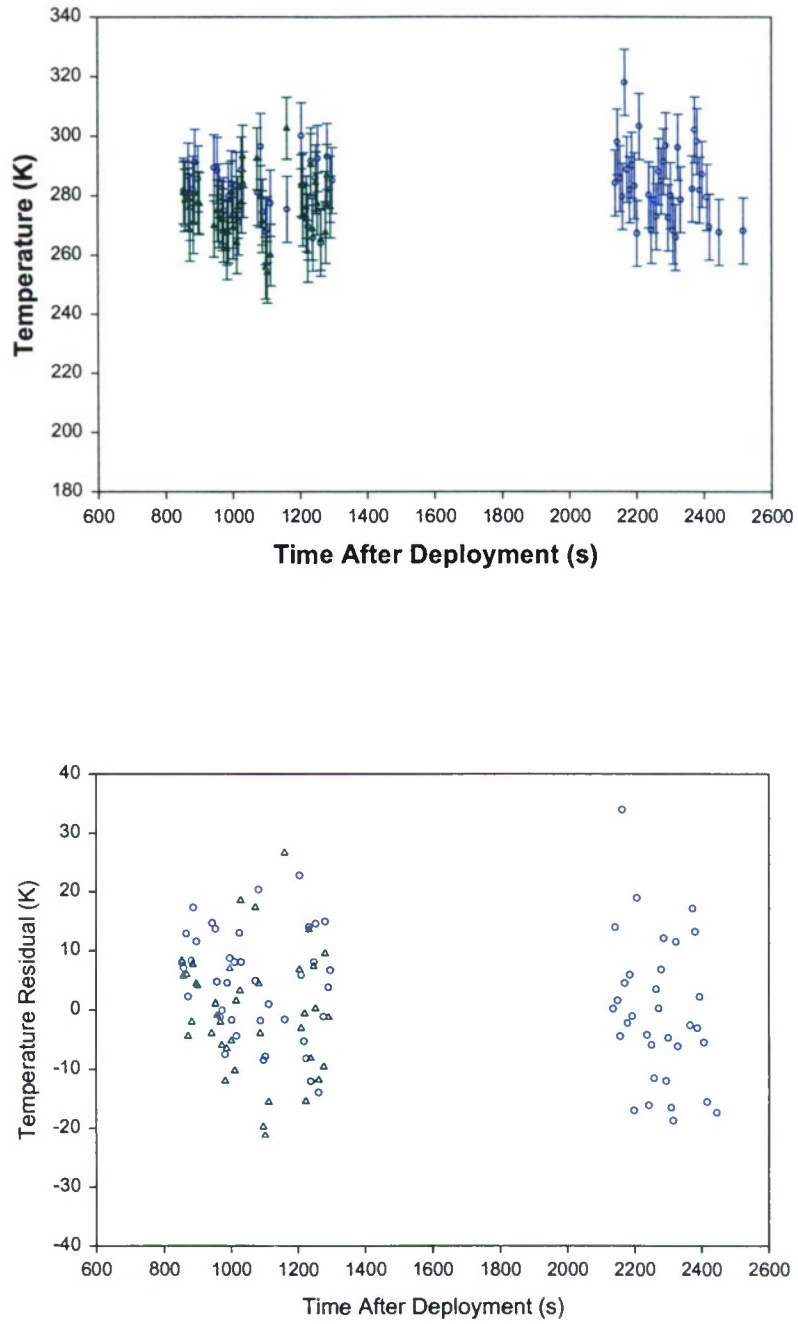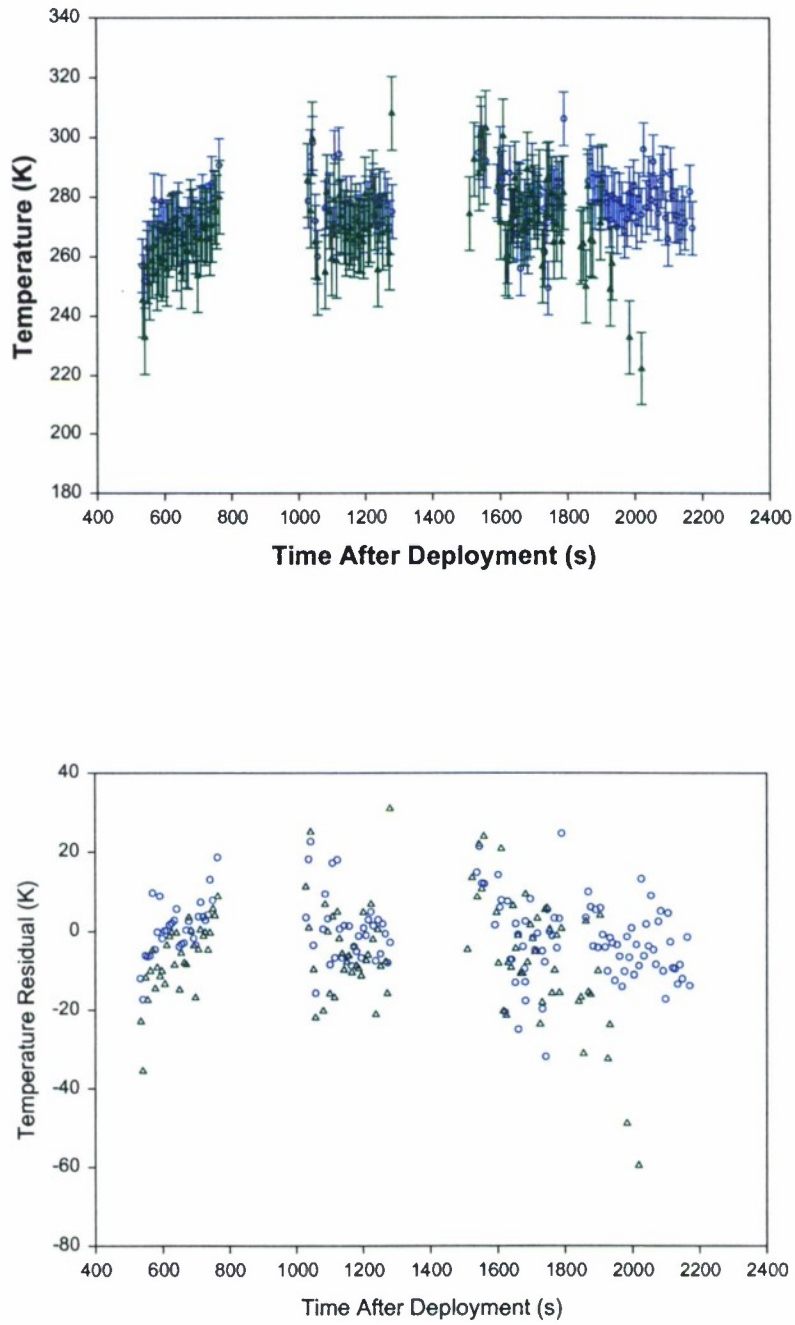
Figure A3. Temperature history (top) and temperature residuals (bottom) for Emissive Reference Sphere #4. Bands A/C are represented by triangles and circles represent bands A/D.

Figure A4. Temperature history (top) and temperature residuals (bottom) for Emissive Reference Sphere #5. Bands A/C are represented by triangles and circles represent bands A/D.

33

APPENDIX B
EMISSIVE REFERENCE SPHERE EMISSIVITY-AREA RESIDUALS

The emissivity-area product calculated from the band A irradiance by the SPIRIT III Data Reduction pipeline for reference sphere 1 (ERS-1) was presented in Section 6 of this report. This appendix presents the band-A εA residuals for all 5 reference spheres. Each plot shows the residual (calculated εA – truth εA) as a function of time after sphere deployment. Three-sigma outliers have been removed from each data set.
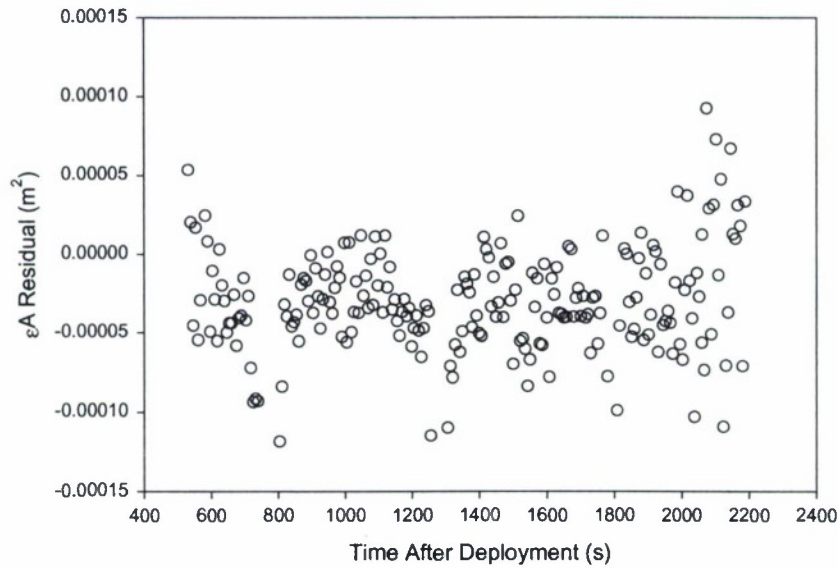
Figure B1. Emissivity-Area product residuals for ERS-1. These data are the differences between the calculated εA and the true εA for the sphere.
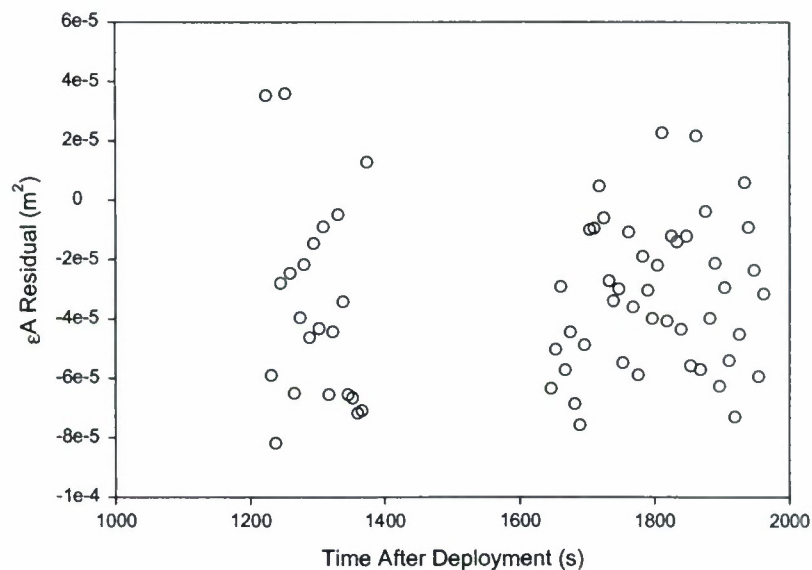
Figure B2. Emissivity-Area product residuals for ERS-2. These data are the differences between the calculated εA and the true εA for the sphere.
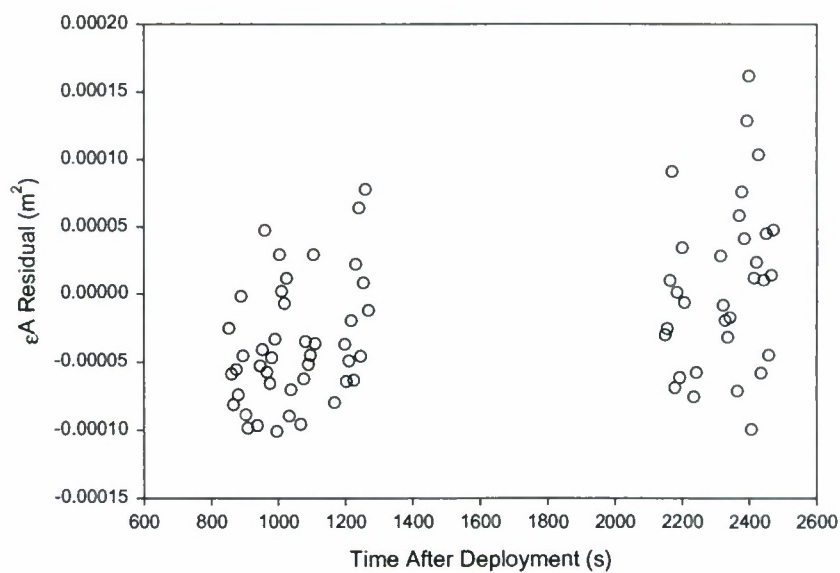

Figure B3. Emissivity-Area product residuals for ERS-3. These data are the differences between the calculated εA and the true εA for the sphere.
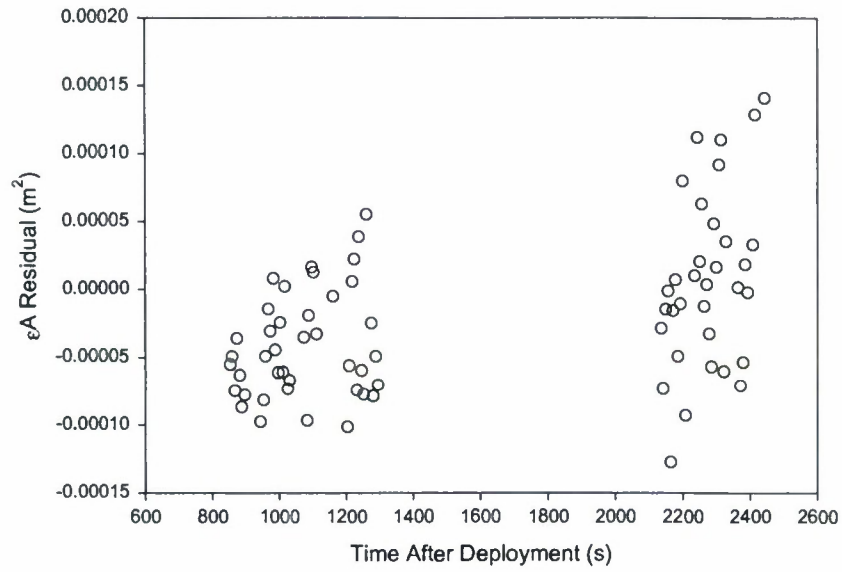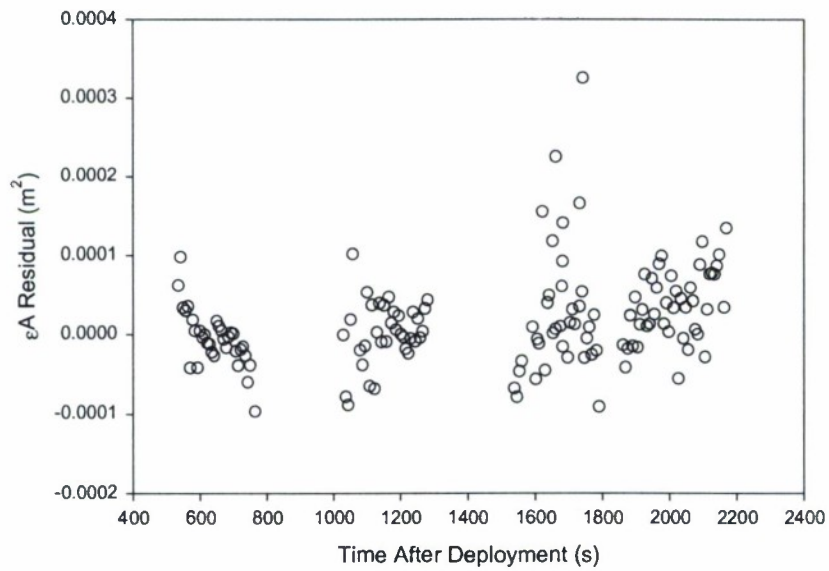
Figure B4. Emissivity-Area product residuals for ERS-4. These data are the differences between the calculated εA and the true εA for the sphere.

Figure B5. Emissivity-Area product residuals for ERS-5. These data are the differences between the calculated εA and the true εA for the sphere.

37

APPENDIX C
ANALYTIC ESTIMATE OF εA BIAS

An analytic estimate of the bias in εA due to biases in range and estimated color temperature is developed. We note that the εA is derived from the definition of brightness temperature as described in Section 6. We repeat Equation (11) here for conveinience:

$$\varepsilon A_i = \frac{\pi R^2 I_i}{\int_0^\infty RSR_i(\lambda)B(\lambda, T_{color})d\lambda} \tag{C1}$$

From simple propagation of errors[23], the fractional error in εA can be written as:

$$\frac{\Delta \varepsilon A}{\varepsilon A} = \frac{2\Delta R}{R} + \left[\frac{-1}{\int_0^\infty RSR_i(\lambda)B(\lambda, T_c)d\lambda} \left(\int_0^\infty \frac{RSR_i(\lambda)B(\lambda, T_c)}{(e^{\frac{hc}{\lambda k T_c}} - 1)} \frac{hce^{\frac{hc}{\lambda k T_c}}}{\lambda k T_c} d\lambda \right) \right] \frac{\Delta T_c}{T_c} \tag{C2}$$

where T_c was used for T_{color} to simplify the notation, i stands for wavelength band, and we assumed that there is no variation in the irradiance (we are interested only in estimating the contribution of range and temperature biases on εA). For range biases only, we neglect the temperature term and note that the fractional error in εA is twice that in range. For temperature bias only, we neglect the range term. The resulting εA bias is shown in Figure C1 as a function of target temperature for a temperature bias of $\Delta T_c = +2\%$. This bias corresponds to a bias of ~6 °K at a target temperature of 280 °K.
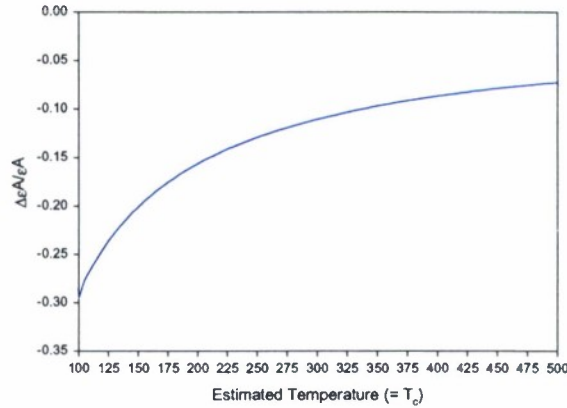

Figure C1. Estimated fractional bias in εA due to positive bias in estimated color temperature.

REPORT DOCUMENTATION PAGE

1. AGENCY USE ONLY (*Leave blank*)	2. REPORT DATE 13 September 2002	3. REPORT TYPE AND DATES COVERED Technical Report

4. TITLE AND SUBTITLE
Calculation of Resident Space Object Color Temperature
and Emissivity-Area from MSX Spirit III Infrared Data:
Emissive Reference Sphere Results

5. FUNDING NUMBERS

C — F19628-00-C-0002

6. AUTHOR(S)

Dr. Richard L. Lambour

7. PERFORMING ORGANIZATION NAME(S) AND ADDRESS(ES)

MIT Lincoln Laboratory
244 Wood Street
Lexington, MA 02420-9108

8. PERFORMING ORGANIZATION REPORT NUMBER

TR-1063

9. SPONSORING/MONITORING AGENCY NAME(S) AND ADDRESS(ES)

Department of the Air Force
ATTN: SMC/MTAG Capt. Eddie Alonso
185 Discoverer Blvd.
El Segundo, CA 90245-4695

10. SPONSORING/MONITORING AGENCY REPORT NUMBER

ESC-TR-99-066

11. SUPPLEMENTARY NOTES

12a. DISTRIBUTION/AVAILABILITY STATEMENT

Aproved for public release; distribution is unlimited.

12b. DISTRIBUTION CODE

13. ABSTRACT (*Maximum 200 words*)

This report discusses the calculation of color temperature and emissivity-area product from resident space object (RSO) observations that were obtained during a series of surveillance experiments carried out with the Midcourse Space Experiment (MSX) spacecraft. During these experiments, simultaneous infrared and visible-band data were collected with the SPIRIT III LWIR infrared radiometer and the Space-Based Visible (SBV) instruments, respectively. Algorithms were developed for the SPIRIT III Data Reduction pipeline which allow calculation of color temperature and emissivity-area product for RSOs given that the RSO was observed in at least two wavelength bands. This report discusses the algorithms and characterizes their accuracy using data taken on five emissive reference spheres that were deployed from the satellite over the lifetime of the SPIRIT III instrument.

14. SUBJECT TERMS

15. NUMBER OF PAGES
46

16. PRICE CODE

17. SECURITY CLASSIFICATION OF REPORT Uclassified	18. SECURITY CLASSIFICATION OF THIS PAGE Unclassified	19. SECURITY CLASSIFICATION OF ABSTRACT Unclassified	20. LIMITATION OF ABSTRACT Same as Report